Mechanism of O₂ diffusion and reduction in [FeFe] hydrogenases

Adam Kubas,[†,‡,@] Christophe Orain,[¶,@] David De Sancho,[§,@]

Laure Saujet,[∥] Matteo Sensi,[¶] Charles Gauquelin,[⊥] Isabelle Meynial-Salles,[⊥] Philippe Soucaille,[⊥]

Hervé Bottin,[∥] Carole Baffert,[¶] Vincent Fourmond,[¶]

Robert B. Best,[#] Jochen Blumberger,[*,†] and Christophe Léger[*,¶]

E-mail: j.blumberger@ucl.ac.uk; christophe.leger@imm.cnrs.fr

[*]To whom correspondence should be addressed

[†]Department of Physics and Astronomy, University College London, Gower Street, London WC1E 6BT, UK

[‡]Institute of Physical Chemistry, Polish Academy of Science, ul. Kasprzaka 44/52, Warsaw, Poland

[¶]Aix Marseille Université, CNRS, BIP UMR 7281, 13402, Marseille, France.

[§]Department of Chemistry, University of Cambridge, Lensfield Road, Cambridge CB2 1EW, United Kingdom; CIC nanoGUNE, Tolosa Hiribidea 76, 20018 Donostia-San Sebastián, Spain and IKERBASQUE; Basque Foundation for Science, Maria Diaz de Haro 3, 48013 Bilbao, Spain

[∥]Institut de Biologie et de Technologies de Saclay IBITECS, SB2SM, F-91191 Gif sur Yvette, France / Institut de Biologie Intégrative de la Cellule I2BC, UMR 9198, CEA, CNRS, Université Paris Sud, F-91191 Gif sur Yvette, France

[⊥]Université de Toulouse, INSA, UPS, INP, LISBP, INRA:UMR792, CNRS:UMR 5504, 135 avenue de Rangueil, 31077 Toulouse cedex 04, France

[#]Laboratory of Chemical Physics, National Institute of Diabetes and Digestive and Kidney Diseases, National Institutes of Health, Bethesda, Maryland 20892-0520, United States

[@]Contributed equally to this work.

Abstract

[FeFe] hydrogenases are the most efficient H_2 producing enzymes; however, inactivation by O_2 remains an obstacle which prevents them being used in many biotechnological devices. Here we combine electrochemistry, site-directed mutagenesis, molecular dynamics and quantum chemical calculations to uncover the molecular mechanism of O_2 diffusion within the enzyme and its reactions at the active site. We find that the partial reversibility of the reaction with O_2 results from the four-electron reduction of O_2 to water. The third electron/proton transfer step is the bottleneck for water production, competing with formation of a highly reactive OH radical and hydroxylated cysteine. The rapid delivery of electrons and protons to the active site is therefore crucial to prevent the accumulation of these aggressive species during prolonged O_2 exposure. These findings should provide important clues for the design of hydrogenase mutants with increased resistance to oxidative damage.

One of the grand scientific challenges facing society is the design of cheap catalysts for efficient production and oxidation of carbon neutral energy carriers such as molecular hydrogen. A very promising perspective in this regard is to harness the catalytic power of NiFe and FeFe hydrogenases, the enzymes that have evolved over millions of years to produce and oxidize H_2.[1] Living microorganisms that express hydrogenases, or purified hydrogenases, could be used in this context; these highly efficient enzymes are also an invaluable source of inspiration for inorganic chemists to design synthetic mimics.

However, a major obstacle to using either type of hydrogenases is their sensitivity to oxidation, and the characterisation of their inactivation by O_2 has become a major field of research.[2] NiFe hydrogenases that naturally resist O_2 have recently been identified[3,4] and attempts to increase the resistance of O_2 sensitive NiFe hydrogenases have been partially successful.[5] A different solution is to incorporate the enzyme into a redox polymer film that provides a self-activated O_2 shield,[6,7] but it is unknown if this strategy can protect the enzyme under conditions of reductive catalysis.

This paper deals with FeFe hydrogenases, which are more active for H_2-production and less inhibited by H_2 than NiFe hydrogenases.[8] Their active site, the "H-cluster", consists of a [$Fe_2(CO)_3(CN)_2$(dithiomethylamine)] subsite[9,10,11,12] covalently bound to a 4Fe4S subcluster. Fig. 1a shows the structure of the bidirectional FeFe hydrogenase 1 from *Clostridium pasteurianum* (*Cp*), a

structural homolog of the FeFe hydrogenase from *Clostridium acetobutylicum* (*Ca*),[9] which covalently binds four FeS clusters in addition to the H-cluster. The enzyme from the photosynthetic organism *Chlamydomonas reinhardtii* (*Cr*) has no cofactor other than the H-cluster.[13] Due to the sensitivity of FeFe hydrogenases to molecular oxygen, understanding the mechanism of O_2 inhibition is a prerequisite for using genetic engineering to increase their O_2-tolerance. This is crucial in the case of the enzyme from *Cr*, since this green alga could be used for biological H_2 photoproduction[14] if its hydrogenases were less inhibited by the O_2 produced by photosynthesis.
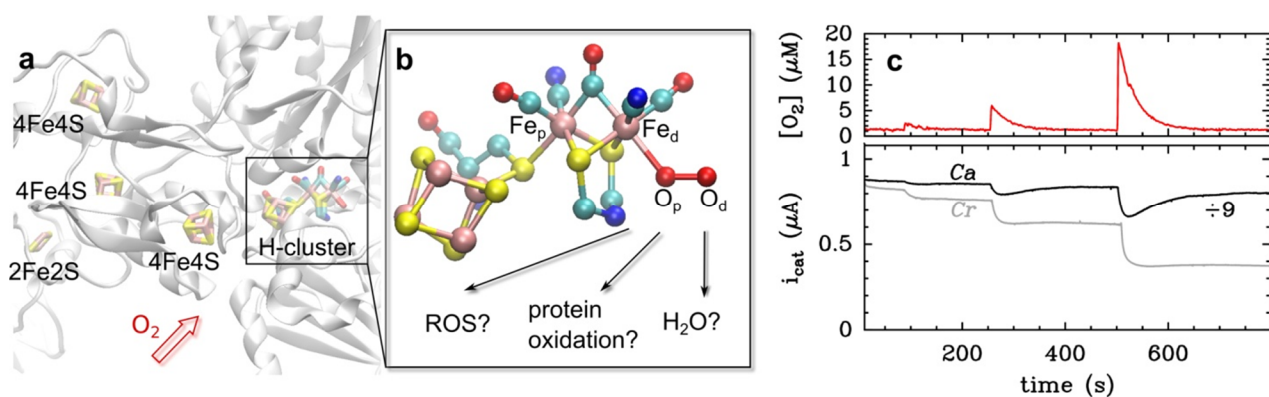

Figure 1. FeFe hydrogenase and the inhibition of this enzyme by O_2. **a**: Crystal structure of FeFe hydrogenase from *Clostridium pasteurianum* (*Cp*, PDB id 3C8Y), a structural homologue of *Ca* FeFe hydrogenase. The protein backbone is shown in cartoon representation and the FeS- and H-clusters in licorice representation. Color code: Fe: pink, S: yellow, O: red, N: blue, C: cyan. **b**: Enlarged view of the H-cluster with O_2 bound to the distal iron, Fe_d, and a nitrogen atom in the dithiomethyl bridge.[9,51,52] Possible reaction products are indicated, ROS refers to reactive oxygen species, e.g. O_2H, H_2O_2 or OH. **c**: *Ca* and *Cr* FeFe hydrogenases behaviour upon exposure to O_2. The top panel shows the instantaneous O_2 concentration, the bottom panel shows catalytic H_2-oxidation current against time for *Ca* (black) and *Cr* (gray) FeFe hydrogenases (*T*= 12 °C, 1 bar H_2, pH = 7, data reproduced from ref 12).

Aerobic inhibition of FeFe hydrogenase involves the diffusion of O_2 through the protein[15] and its initial attack on the vacant site on the Fe that is remote from the cubane (the so-called distal iron, Fe_d, see Fig. 1b).[16,17,18,19,20] Quantum chemical calculations rule out outer-sphere electron transfer to O_2,[20] but what happens after O_2 attachment is unclear. According to X-ray absorption measurements, exposing the enzyme from *Cr* to O_2 damages the 4Fe4S subcluster; this suggested that O_2 binding to Fe_d results in the formation of a reactive oxygen species (ROS) that diffuses towards the 4Fe4S subcluster and destroys it.[18,21] According to the DFT studies of Reiher[22,23] and

Pachter,[24] this ROS could be the OOH radical or H_2O_2. However, the mechanism in refs 18 and 21 conflicts with a recent report according to which the O_2-damaged enzyme from *Cr* harbors an intact 4Fe4S subsite and no 2Fe subcluster, and the observation that the O_2-damaged enzyme is repaired upon insertion of a synthetic analogue of the 2Fe subcluster.[25]

Protein film electrochemistry (whereby the enzyme is adsorbed onto an electrode and electron transfer is direct) has been useful for characterizing the kinetics of aerobic inhibition of hydrogenases, because the activity can be recorded as a current while the enzyme is exposed to controlled "bursts" of oxygen.[16] Fig. 1C shows the response of *Ca* and *Cr* hydrogenases to pulses of O_2. The activity of *Ca* hydrogenase is mostly recovered after a brief exposure to O_2, but the enzyme is irreversibly inactivated by a prolonged exposure to O_2. The enzyme from *Cr* is inhibited more strongly and less reversibly than that from *Ca*, but we have recently demonstrated that the mechanism of inhibition for both enzymes is described by the same kinetic scheme:[16]

$$\mathbf{A} \underset{k_a}{\overset{k_i[O_2]}{\rightleftharpoons}} \mathbf{I} \overset{k_3}{\rightarrow} \mathbf{D} \tag{1}$$
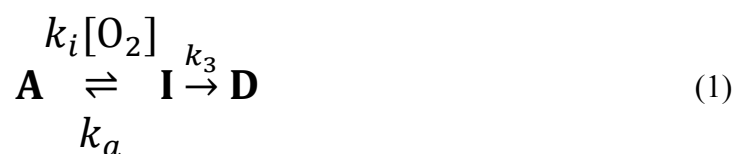
The active enzyme "A" reacts with O_2 (second order rate constant k_i) to form an inactive species "I" that either reverses to A (first order rate constant k_a) or irreversibly transforms into a dead-end, irreversibly inactivated species "D" (k_3).

Here, we examine how the above-defined rate constants depend on electrode potential, pH, replacement of H_2O with D_2O, and on protein mutations. We combine this experimental information with the results of theoretical chemistry calculations[26] – molecular dynamics (MD) simulation and Markov state modelling of O_2 diffusion in the enzyme to the active site, as well as density functional theory (DFT) calculations for the characterization of the reaction products – to deduce the molecular mechanism of each step in the above kinetic scheme.

Results

We used the method described in ref. 16 to examine how the kinetics of inhibition of FeFe hydrogenase by O_2 depends on the experimental conditions. Fig. 2 shows raw electrochemical data, and Fig. 3 summarizes the changes in k_i, k_a and k_3 (defined in eq. 1) against electrode potential (E), for experiments performed in H_2O at 3 pH values, and one set of experiments performed with the enzyme oxidizing D_2 in D_2O at pD 7.
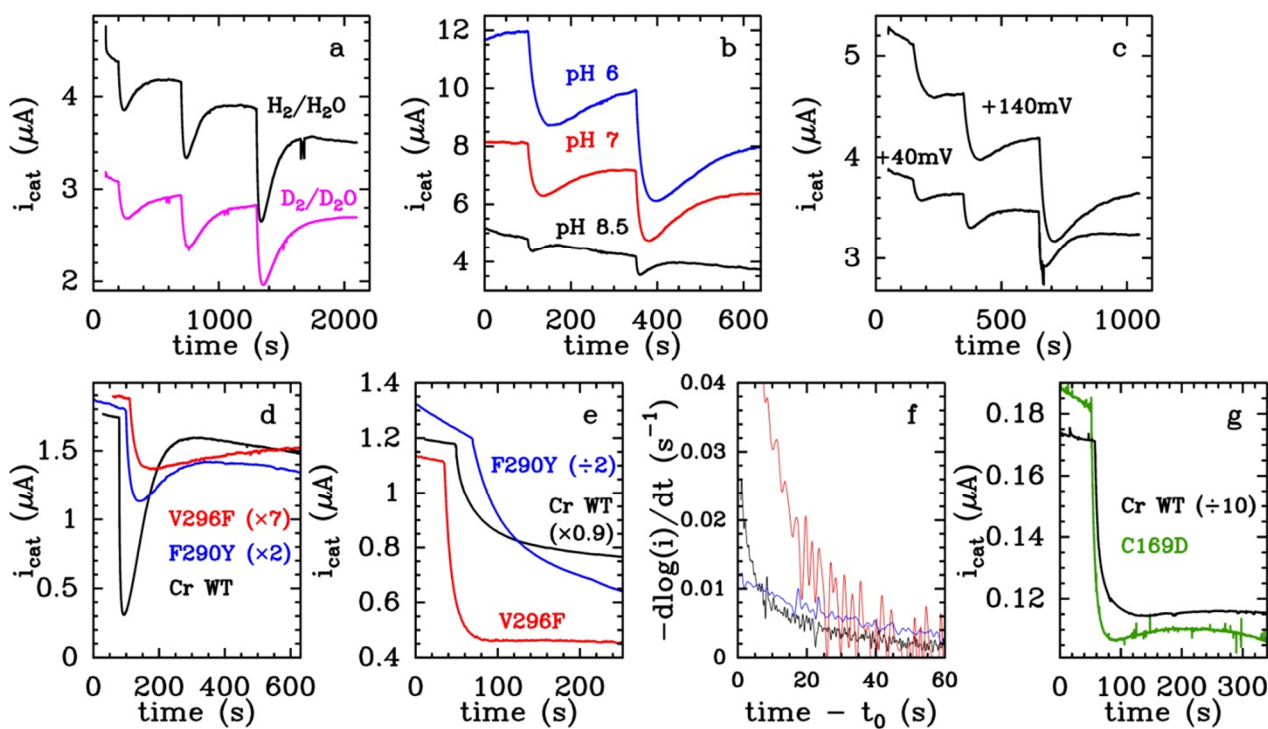
Figure 2. Change in catalytic H_2-oxidation current against time.n these experiments, *Ca* (panels a-c) or *Cr* (panels **d-g**) FeFe hydrogenases were exposed to "bursts" of CO (panel d) or O_2 (all other panels). The data were not corrected. The "×" and "÷" indicate normalization factors. In these experiments, the absolute magnitude of the current should not be interpreted because it depends on the electroactive coverage that is both unknown and variable. **a**: Effect of H/D exchange on the inhibition of WT *Ca* FeFe hydrogenase by O_2 at pH or pD = 7.1. **b**: Effect of pH on the inhibition of WT *Ca* FeFe hydrogenase by O_2. **c**: Effect of electrode potential on the inhibition of WT *Ca* FeFe hydrogenase by O_2. **d**: Effect of F290Y and V296F substitutions on the inhibition of *Cr* FeFe hydrogenase by CO. **e**: Effect of F290Y and V296F substitutions on the inhibition of *Cr* FeFe hydrogenase by O_2. **f**: the same data as in panel **e** but in a plot of $-d(\log(i))/dt$ against the time after the injection of O_2, giving the instantaneous rate constant of inactivation at the time of injection of O_2.[27] **g**: Effect of C169D substitution on the inhibition of *Cr* FeFe hydrogenase by O_2. See Supplementary section S5.1 for detailed experimental conditions.
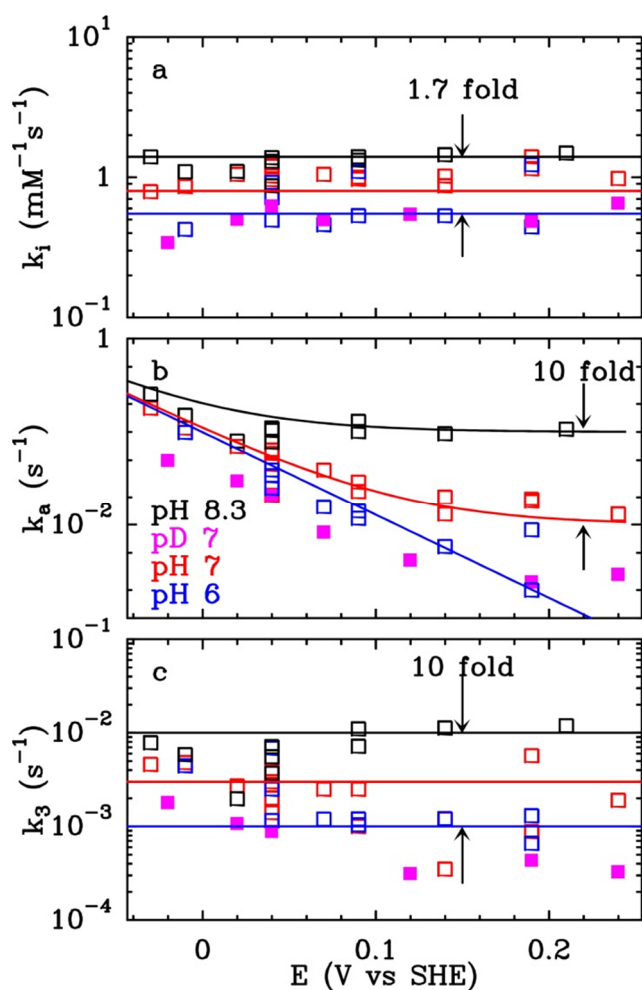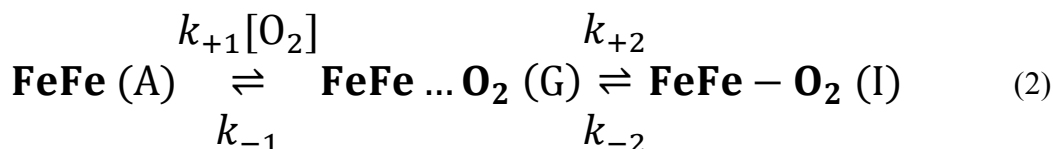
Figure 3. Potential dependence of the three rate constants defined in eq. 1. The rates constants were measured in experiments where *Ca* FeFe hydrogenase is inhibited by O_2 at pH 6 (blue), 7 (red) and 8.3 (black), and pD 7 (pink, see Methods). All at T = 12 °C, 1 bar H_2 or D_2. The bimolecular rate constant of the initial O_2 binding step, k_i, is independent of E and pH, and the rate of formation of the dead-end species, k_3, only depends on pH. The horizontal lines in panels **a** and **c** are a guide to the eye at k_i=1.4, 0.8 and 0.55 in panel a and k_3=0.01, 0.003 and 0.001 in panel c. Two pathways (the rate constants of which add up) contribute to reactivation: the lines in panel **b** are the sum of a pH-dependent constant (0.1 at pH 8.3 and 0.01 at pH 7) and a pH-independent function that is proportional to exp(-FE/2RT).

Initial O$_2$ attack (rate constant k_i)

Fig. 3A shows that the second order rate constant of O$_2$ binding, k_i, is independent of E and pH (it increases less than 2-fold over 2 pH units), with no significant isotope effect, consistent with k_i simply describing the diffusion of O$_2$ through the protein and its binding at the active site. The rate k_i of conversion from A to I in eq. 1 can be calculated from the rate constants in the following scheme:[28,29]

$$\textbf{FeFe (A)} \underset{k_{-1}}{\overset{k_{+1}[O_2]}{\rightleftharpoons}} \textbf{FeFe} \ldots \textbf{O}_2 \textbf{ (G)} \underset{k_{-2}}{\overset{k_{+2}}{\rightleftharpoons}} \textbf{FeFe} - \textbf{O}_2 \textbf{ (I)} \qquad (2)$$

Above, k_{+1} is the second-order rate constant for the diffusion of O$_2$ from the solvent to the active site and k_{-1} is the first-order rate constant for the diffusion in the opposite direction. In the resulting state G (for "Geminate"), O$_2$ is in the active site pocket but it is not yet chemically bound to the active site. The formation and breaking of the chemical bond is described by the first-order rate constants k_{+2} and k_{-2}, respectively. As shown in supplementary section S1 and refs 26, 28 the measured rate constant k_i is related to the rate constants in eq. 2 by:

$$k_i = \frac{k_{+1}k_{+2}}{k_{-1} + k_{+2}} \qquad (3)$$

We have previously investigated the chemical binding of O$_2$ to the H-cluster, and determined a binding free energy of -7.1 kcal/mol and an activation free energy of 12.9 kcal/mol from quantum chemical calculations;[20] this gives $k_{+2} = 2.2 \times 10^3$ s^{-1} and $k_{-2} = 1.4 \times 10^{-2}$ s^{-1} at T=298 K. The value of k_{+2} is three orders of magnitude larger than the experimental (pseudo-first order) inhibition rate at typical ligand concentrations of 1 mM, $k_i \times 1$ mM, indicating that intraprotein diffusion is an essential part of the binding kinetics.

We obtained the pathways of intraprotein O$_2$ diffusion from atomistic MD simulations of *Cp* FeFe hydrogenase (for which a high-quality X-ray structure is available[9]) in the presence of O$_2$ molecules. We calculated the corresponding diffusion rate constants $k_{\pm1}$ by careful analysis of the atomistic dynamics based on a Markov state model (MSM).[30,31] In the MSM, the access of O$_2$ to the H-cluster is described as a series of discrete jumps, from the solvent to protein cavities, and between protein cavities. The dynamics of hopping between these cavities is given by a kinetic master equation with transition rate constants obtained from the MD data (see Methods and Supplementary section S2 for details). Fig. 4a shows the structure of the *Cp* FeFe hydrogenase, the microstates obtained from the MSM, and the two pathways (1 and 2) with the highest diffusive flux towards the active site. The dominant path (1) was also identified by Schulten and co-workers as the most

important access tunnel ("pathway A" in ref. 15). Diffusion along pathway 2 is less likely to occur, as the gas molecule needs to get around the sidechain of F417 (see Fig. 4b and S3). The bottleneck for ligand diffusion along the dominant pathway 1 is the last transition, involving the jump from site 7 to the geminate site. Only when thermal fluctuations increase the distance between Cys299-Pro324 and Cys299-F417 is the passage of O_2 into the active site possible (see Fig. 4c), but these events are rare. From the MSM we obtain the values k_{+1}= $3.0\pm1.8\times10^3$ $s^{-1}mM^{-1}$ and k_{-1}= $7.7\pm0.3\times10^7$ s^{-1} (see Fig. S6b). Combining k_{+1}, k_{-1} and k_{+2} according to eq. 3, we calculate k_i=$8.6\pm5.1\times10^{-2}$ $s^{-1}mM^{-1}$. The 13-fold difference from the measured k_i (1.1 $s^{-1}mM^{-1}$) represents good agreement, considering that besides the statistical uncertainties quoted, each of the contributing rate coefficients k_{+1}, k_{-1} and k_{+2} includes errors due to approximations and inaccuracies in the underlying computational models.

The molecular-scale picture of the diffusion process obtained from MD simulation of the *Cp* hydrogenase is supported by the experimental results in Fig. 2d, showing the binding of the competitive inhibitor CO to WT and mutant forms of the structurally homologous *Cr* hydrogenase. (CO binds reversibly to Fe_d under oxidizing conditions.[32]) Replacing V423 (Cp numbering, Cr V296) (Fig. 4b) with a phenylalanine, or F417 (Cp numbering, Cr F290) with a tyrosine, significantly decreases the rates of CO binding and release: from k_i^{CO} = 60 ± 15 $s^{-1}mM^{-1}$ and k_a^{CO} = 0.025 ± 0.006 s^{-1} in the WT, to 6 ± 2 $s^{-1}mM^{-1}$ and 0.0014 ± 0.0002 s^{-1} (n = 3 independent determinations) in *Cr* V296F and 7 ± 2 $s^{-1}mM^{-1}$ and 0.008 ± 0.001 s^{-1} (n = 3) in *Cr* F290Y, all at 30 °C, pH 7, E = -158 mV. Note that *Cr* F290 was mistakenly numbered F234 in ref. 33. We also observed that the *Cr* F290W mutant has no activity. Explicit MD simulations of the *Cp* V423F and *Cp* F417Y mutants (see Fig 4b and Supplementary Information) predict a slowdown in the last transition into the geminate site, resulting, respectively, a ~2-fold and 100-fold decrease in the k_{+1} rate. Hence, experiment and simulation concur that the transition from site 7 to the geminate site is a key step in ligand diffusion to the active site.

The CO data in Fig. 2d inform on O_2 intramolecular diffusion because there is evidence that, at least in the case of NiFe hydrogenase, CO and O_2 use the same pathway to access the active site.[28] However, eq. 3 shows that intramolecular diffusion is not the only factor that determines the rate of reaction with O_2. Fig. 2e shows the reaction of Cr WT FeFe hydrogenase and the two mutants with oxygen. Figure 2f shows the corresponding plot of $d(\log(i))/dt$ against time, which can be extrapolated to the time of O_2 injection to estimate the pseudo-1st order rate constant of reaction with O_2.[27] The reaction of F290Y with O_2 is half as fast as for the WT, consistent with the observation in Fig. 2d that the F290Y mutation slows access to the active site. Surprisingly, the reaction of the V296F mutant with O_2 is about 2.5-times faster than with the WT, despite CO access

to the active site being slower (Fig. 2d). However, Supplementary Fig. S12 shows that the *anaerobic* oxidative inactivation mechanism of the V296F mutant is qualitatively different from that of the WT (the chemistry is different, not just the rates), suggesting that the mutation affects not only the diffusion kinetics, but also the reactivity of the active site in a manner that appears to increase the rate of reaction with O_2, and compensates for slower intramolecular diffusion.
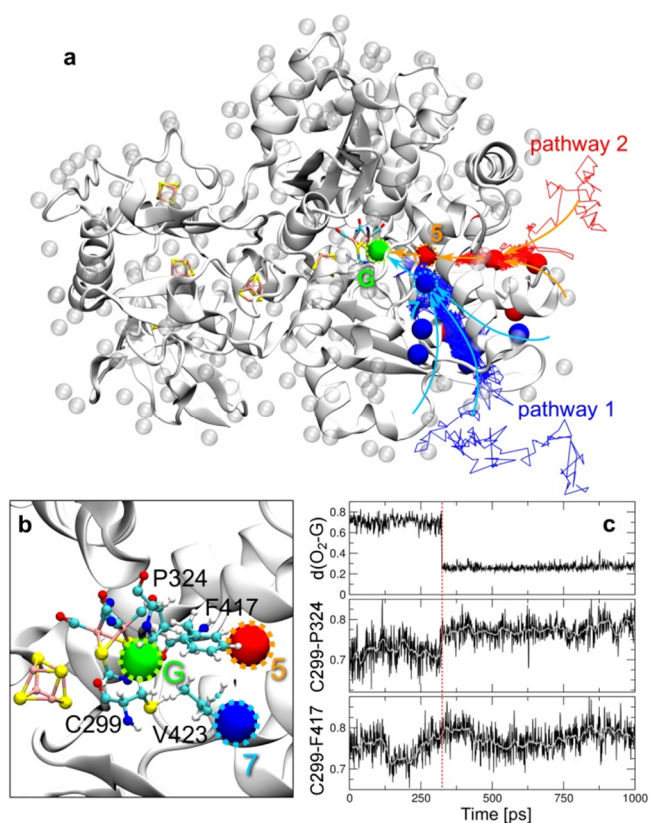

Figure 4. Markov state model for O_2 diffusion into *Cp* hydrogenase. **a**: Location of gas molecule microstates identified from the MD simulations (transparent spheres) overlaid on the structure of *Cp* hydrogenase (white). Atomic detail is shown only for the inorganic clusters. Red and blue solid spheres mark the microstates that are involved in the two paths (1 and 2, in blue and red) to the H-cluster. Microstates 5 (red with orange dotted line) and 7 (blue, with cyan dotted line) are those directly connected to the geminate site (G, green), as derived from flux calculations. Example paths arriving through pathways 1 and 2 are shown as blue and red lines, respectively. **b**: Zoom into the vicinity of the H-cluster. The geminate, 5 and 7 sites are shown colour coded as in **a**. **c**: Distance between key residues (shown in panel **b**), that block the access to the active site, as obtained from low force pulling simulations. Note the increase in distance between the sidechains of Cys299 and those of Pro324 (middle panel) and Phe417 (bottom panel) at about 320 ps (red dashed line), facilitating the transition of an O_2 molecule from microstate 7 to the geminate site G.

Reactivation (k_a)

The rate constant k_a in eq. 1 corresponds to the transformation of the O_2-adduct into an active form of the enzyme. As shown below, this reaction is more complex than the mere release of bound O_2. Indeed, reactivation is slowed by replacing H_2O and H_2 with D_2O and D_2 (Fig. 2a, kinetic isotope effect (KIE) in the range 2.4 – 4 at $T = 12\ °C$, depending on potential), and the value of k_a is strongly dependent on pH and electrode potential E (Fig. 2b and c). Moreover, the observation in Fig. 3b that k_a decreases exponentially as E increases and then levels off at high E provides unambiguous evidence that two distinct processes contribute to the reactivation: one that is triggered by a reduction (hence the sigmoidal increase in k_a as E decreases, the observed exponential variation being the foot of this sigmoid) and one that is non-redox and predominates at high E and high pH. The value of k_a in Fig. 3b is the sum of the two corresponding reactivation rates.

We first consider the non-redox reactivation, whose rate is independent of potential and increases ten-fold per pH unit between pH 6 and 8 (Fig. 3b). This shows that the non-redox reactivation occurs only from the basic form of a species whose protonation/deprotonation is fast compared to k_a. Theoretical calculations (see Supplementary section S3) suggest that the two protonation states are Fe_d-O_2H^+ and Fe_d-O_2 and that protonation occurs via a neighbouring Cys that is part of a proton transfer chain connecting the active site to the solvent (Cys299 in *Cp* hydrogenase, Cys169 in the *Cr* enzyme).[23,34,35,36,37] In the alkaline limit where $[Fe_d$-$O_2H^+] \ll [Fe_d$-$O_2]$, the computed $k_a = k_{-2} = 1.4 \times 10^{-2}\ s^{-1}$, compares favourably with the experimental estimate of $k_a > 1.0 \times 10^{-1}\ s^{-1}$ (see Supplementary section S3 for further discussion).
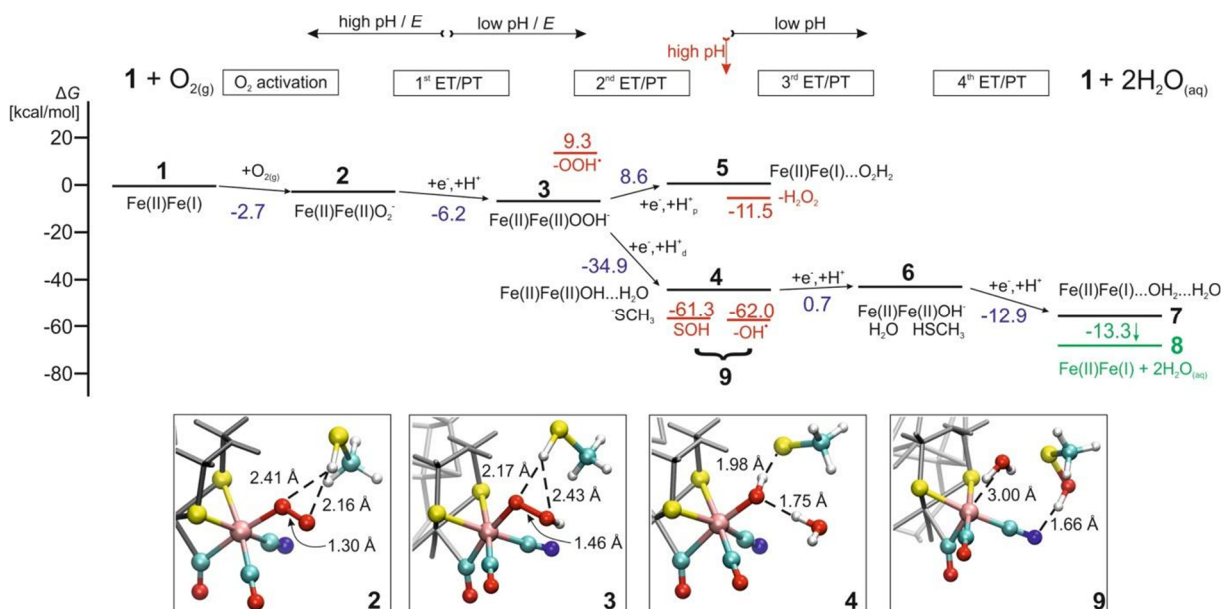
Figure 5. Graphical representation of the relative free energies of the most important states (**1 – 9**) involved in oxygen reduction to water at the active site of the FeFe hydrogenase. The free energies, shown for pH=7 relative to the SHE, were obtained from DFT calculations on large active site models, as explained in detail in Supplementary section S4. State **1** is equivalent to species "A" in eq. 3. For structures **2, 3**, **4**, **9**, the most important interatomic distances are shown in the respective insets. The first coordination sphere of the distal iron atom is presented in ball and stick representation (color code: Fe pink, O red, C turquoise, N dark blue, S yellow, H white).

We now turn our attention to reductive reactivation, which dominates at low E (Fig. 3b). We propose that the reactivation process is the reduction of bound oxygen to a species whose dissociation from the active site gives back the active state. This hypothesis is confirmed by extensively validated theoretical calculations (see Supplementary section S4) for consecutive ET/PT coupled reduction of O_2 bound to the active site (Fig. 5). Calculations suggest that the 4 electron/4 proton reduction of O_2 is possible without formation of high energy intermediates, and the species dissociating from the active site is indeed water. During the first ET/PT step (**2→3**, -2.7 kcal/mol) the O-O bond length is elongated from 1.30 to 1.46 Å, which is best interpreted as a change from a superoxide to a hydro-peroxide species, see inset **3** in Fig. 5. The second step may proceed via two pathways. The proton can attach either to the proximal Fe-bound oxygen to form hydrogen peroxide (**3→5**) or to the distal oxygen atom, upon which the O-O bond breaks and the first water molecule is formed (**3→4**). We found that the formation of water is highly exothermic (-34.9 kcal/mol) and strongly preferred over the endothermic formation of hydrogen peroxide (+8.6 kcal/mol). The proximal oxygen atom easily abstracts the hydrogen atom from Cys299, which results in a shift of electron spin density from oxygen to sulfur. The same proton transfer reaction has been discussed in

11

ref. 23. The sulfur atom of Cys299 now serves as a hydrogen bond acceptor, while the newly formed water molecule stabilizes the Fe-bound hydroxy group by hydrogen bonding, see inset **4** in Fig. 5. In the third step (**4→6**), which is mildly uphill (+0.7 kcal/mol), the sulfur atom is re-protonated and the Fe-bound hydroxy radical is reduced to OH⁻. Finally, in the fourth step (**6→7**, -12.9 kcal/mol) the Fe-bound hydroxide is reduced to water and the di-iron site returns to its initial redox state.

The irreversible formation of dead-end species (k_3)

In the kinetic model, the partial irreversibility of the reaction with O_2 is accounted for by the irreversible transformation of the O_2 adduct, with a first order rate constant k_3. Fig. 3c shows that the value of k_3 is independent of E and increases about ten-fold over two pH units (Fig. 2b shows that the inhibition is more reversible at *high* pH, but that is because k_a is greater (cf Fig. 3b) and the O_2 adduct is therefore short lived). Replacing H_2O with D_2O decreases k_3 five-fold. These observations suggest that k_3 is the rate of the non-redox transformation of one of the species shown in Fig. 5.

The conversion of **4** to **6** is the least exergonic step in the reduction of O_2; state **4** may therefore be a bottleneck for water reduction and the starting point for the irreversible formation of various dead-end products. Indeed, calculations reveal that the Fe-bound hydroxy radical can readily attack the deprotonated sulphur atom of Cys299 to form sulphenic acid (inset "**9**" in Fig. 5, -14.0 kcal/mol). The latter is strongly stabilised by a hydrogen bond to the CN⁻ ligand. Alternatively, the dissociation of the OH radical from the distal iron into the active site pocket is also energetically favourable by -14.7 kcal/mol; this highly reactive species could readily oxidize either the H-cluster or surrounding protein residues.[23]

Our proposal that Cys299-SOH and/or free OH radicals are involved in the irreversible inactivation is further supported by the following observations: (i) The formation of Cys299-SOH requires Cys299 to be deprotonated, consistent with the observed increase in k_3 when the pH is increased, and the observed KIE. Besides, an increase in pH makes the 3rd ET/PT step even more endothermic, leading to an increase in concentration of "**4**" and eventually of dead-end product. (ii) Swanson et. al. have observed the oxidation of Cys169 (Cys299 in the enzyme from *Cp*).[25] (iii) The replacement of Cys169 with Asp in the *Cr* enzyme,[38] which has no effect on the spectroscopic signatures of the H-cluster,[39] decreases the value of k_3 about ten-fold, from $k_3 = 24 \pm 3 \times 10^{-3}$ s⁻¹ in the WT to $21 \pm 8 \times 10^{-4}$ s⁻¹ in the C169D mutant (ref. 16 and Fig. S11, see Supplementary section S5 for details). Fig. 2d confirms that the inhibition of the C169D mutant is significantly more reversible than that of the WT enzyme.

Discussion

Fig. 6 summarizes our proposed mechanism of aerobic inactivation of FeFe hydrogenase, including diffusion of O_2 from the solvent, O_2 binding at the active site and the reactions that follow.

Our conclusion from MD calculations that amino acid side chains along the pathway shown in Fig. 4a determine the rates of diffusion of O_2 to the active site is supported by the observation that the V296F and F290Y mutations in *Cr* hydrogenase strongly decrease the rates of binding and release of the competitive inhibitor CO. We found that the rate of inhibition by O_2 of WT FeFe hydrogenase (k_i) is the *product* of two parameters, the ratio k_{+1}/k_{-1} and the chemical binding rate k_{+2} (cf eq. 3, $k_{-1} \gg k_{+2}$). Both ligand diffusion into the active site (k_{+1}) and chemical bond formation (k_{+2}) occur on the 0.1-1 millisecond time scale, but the observed inhibition rate is about 4 orders of magnitude slower, because $k_{+1}/k_{-1} \approx 10^{-4}$ mM^{-1}. This also means that a mutation that decreases both k_{+1} and k_{-1} is expected to slow O_2 inhibition only if it makes k_{-1} lower than k_{+2} (cf eq. 3), as observed previously in a series of NiFe hydrogenase channel mutants.[24]
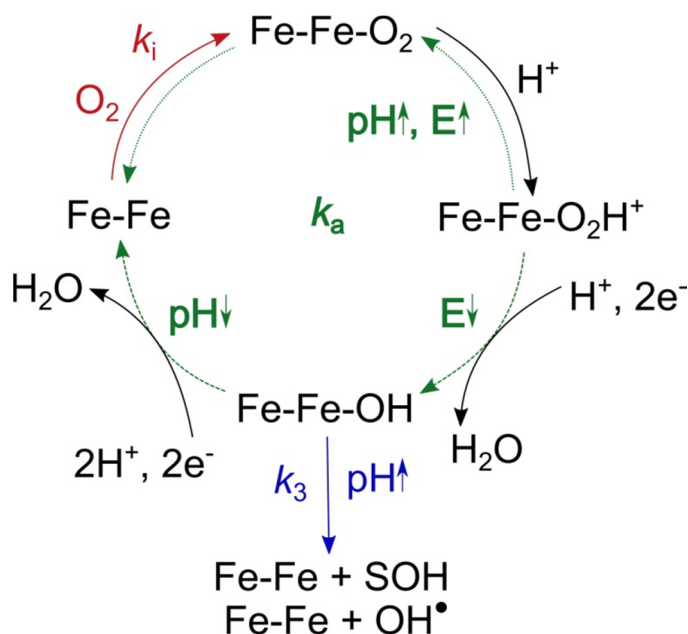

Figure 6. Proposed mechanism for aerobic inhibition of FeFe hydrogenase. The binding of O_2 with rate constant $k_i \times [O_2]$ is indicated in red, the two paths that contribute to the rate constant of reactivation k_a are shown in green. The re-activation path that dominates at high pH and high electrode potential E is indicated by dotted arrows and the re-activation that dominates at low pH and low potential is indicated by dashed arrows. The reaction with rate constant k_3, which makes the inhibition partly irreversible, is depicted in blue.

The partial reversibility of the reaction with O_2 (Fig. 2 and ref. 16) could not be detected in experiments where the enzyme was exposed to a constant concentration of O_2,[18,40] and as a consequence, all previous computational studies of the inhibition of hydrogenase have placed their emphasis on explaining the irreversibility of the reaction. In the light of experimental results showing that O_2 inhibition is reversible (this work and refs 16, 17), a major change of paradigm is required as well as new theoretical calculations that can explain our results on a molecular scale. We have shown that the reactivation results from the combined effects of the release of O_2 and its four-electron four-proton reduction to water (Fig. 6), consistent with recent evidence for O_2 reduction by synthetic analogues of the H-cluster.[41] However, with less than one pmol of enzyme on the electrode and a rate constant of reactivation (O_2 reduction) of about 3×10^{-2} s^{-1}, only a few pmol of H_2O are formed during a 100 s exposure to O_2; using mass spectrometry to detect the reduction of O_2 to H_2O (as in e.g. refs 6, 42) is therefore not possible.

According to our calculations, no high energy intermediate is formed en-route to water formation. By contrast, the formation of hydrogen peroxide requires an endothermic ET/PT step and is therefore unlikely. The two-electron, two-proton reduced state (**4** in Fig. 5) can readily interconvert to produce harmful OH radicals, which could be responsible for H-cluster degradation as observed previously,[18,25] or to hydroxylate the neighbouring cysteine residue, consistent with recent crystallographic evidence.[25] Since this residue is involved in proton transfer from the active site,[43,44] its oxidation alone should be enough to make the enzyme inactive. That irreversible damage follows the two-electron/two-proton reduction of O_2 is consistent with the observation that enzyme lyophilization (which suppresses the source of protons) protects from O_2.[45]

We conclude that the resistance of FeFe hydrogenases to O_2 is largely dependent upon the availability of the electrons that are required for completely reducing the attacking O_2 to water, as recently suggested by Reiher et al.[23] This reaction – which may be physiological, considering the observation that FeFe hydrogenase can be up-regulated in response to oxidative stress[46] – also allows certain NiFe hydrogenases to resist O_2;[2-,3,4,42,47,48] O_2 reduction by NiFe hydrogenases uses electrons produced upon H_2 oxidation and requires the presence of a peculiar FeS cluster that is near the NiFe active site. Considering FeFe hydrogenases, the four electrons required cannot be produced at the H-cluster after O_2 binding and must originate externally. When the enzyme is adsorbed onto an electrode, as occurs in our experiments and in many situations where one seeks to use hydrogenases as a supported catalyst, the electrode functions as an electron reservoir. However, "electron poor" conditions have been used in XAS and X-ray crystallography investigations of the structure of the degradation products,[18,25] with the enzyme in the oxidized state and no H_2 or any

electron donor (although we note that X-rays can sometimes reduce inorganic active sites[49]). If the O_2 reduction cycle that we described cannot proceed due to a lack of electrons, the O_2 adduct **2** may oxidize either the amino acids around the active site, or the H-cluster of other proteins in solution (in an intermolecular reaction). Differences in proton/electron availability may account for some of the variability as to the nature of the degradation products described in the literature,[18,25] when FeFe hydrogenases are exposed to O_2.

We showed that side chain fluctuations, availability of electrons and protons, and the presence of ionizable protein residues in the active site pocket all contribute to defining the O_2 sensitivity of FeFe hydrogenase. We identified the two electron-two proton reduced state as a critical branching point for the formation of water *vs* reactive oxygen species, and revealed key residues that are likely to control the access of O_2 to the H cluster. We observed that substitutions of these residues affect the diffusion rates and the kinetics of anaerobic inactivation, similarly to the valine that gates the substrate access channel in NiFe hydrogenase.[5,28]

Two lines of investigations are worth pursuing in future work. First, the screening of effects of all possible substitutions at positions 169, 290 and 296 (*Cr* numbering) using both electrochemistry and MD simulation, with the aim to restrict O_2 access to the active site and slow the formation of the dead-end species. Second, the systematic search for mutations that accelerate the third ET/PT step (transformation **4→6** in Fig. 5a) using electrochemistry and QM calculations, to eliminate likely bottlenecks for O_2 reduction. The reason the enzyme from *Ca* forms the dead-end species much more slowly than the enzyme from *Cr*[16] should also be investigated; this may be related to the presence of a chain of auxiliary FeS clusters that may help deliver electrons to the active site of the clostridial enzyme.

Methods

Biochemistry and molecular biology

The methods for the purification of the two WT enzymes and *Cr* F290Y hydrogenase have all been fully described previously.[33] (Residue F290 was mistakenly numbered 234 in ref. 33.) The production and electrochemical characterization of the C169D, F290W and V296F mutants are described in Supplementary Information.

Electrochemistry

All potentials are quoted with respect to the standard hydrogen electrode (SHE). The method for measuring k_i, k_a and k_3 has been fully described in ref. 16. In short, the method consists in performing anaerobic experiments (voltammetry and chronoamperometry) to determine all the

parameters that define the *anaerobic* inhibition of the enzyme under oxidizing conditions,[33] then recording the response of the enzyme to repeated exposure to O_2 while monitoring the O_2 concentration, and fitting a model based on eq. 1 to these data, adjusting only the values of k_i, k_a and k_3, all other parameters being fixed to their independently determined values. For determining the isotope effects, the pD was measured with a glass electrode using the correction pD = 0.4+pH meter reading.[50] With hydrogenase on the electrode, the open circuit potential in experiments carried out at pH 7 under one atm. of H_2 was within 10 mV of the value at pD 7 under 1 atm. of D_2. The electrochemical data were analyzed using the new home-made, portable, open source program QSoas (www.qsoas.org).[58]

Molecular dynamics

We have used the Gromacs software package[51] to run atomistic molecular dynamics (MD) simulations of *Cp* hydrogenase (PDB 3C8Y[9]) in explicit water. Simulations were run using an optimized force field for both protein[52] and waters,[53] and a published set of parameters for the inorganic clusters,[54] and in presence of 50 O_2 molecules (see further details in Supplementary section S2). We have analyzed the simulation trajectories to construct a Markov state model (MSM), using the same methodology as described before.[31] Using this approach the dynamics of the gas molecules as they diffuse within the protein is described by a rate matrix **K**, containing rate coefficients k_{ji} corresponding to transitions between pairs of microstates i and j. These microstates are defined from pockets within the protein frequently populated by the O_2 molecules. In our extensive equilibrium MD runs, the gas molecules did not sufficiently sample transitions corresponding to the binding to the geminate site (G). We hence combined the equilibrium rate matrix with rate constants for the $i{\rightarrow}G$ process obtained from pulling simulations from multiple initial states. The rate coefficients k_{Gi} at zero force were derived from a kinetic theory for force induced transitions.[55] The combination of the MSM and fitted rates at zero force has been validated in our previous work.[30] From the rate matrix we obtain the binding (k_{+1}) and dissociation (k_{-1}) rate constants as described before.[30] We use the Berezhkovskii-Hummer-Szabo method[56] to estimate fluxes from the solvent to the geminate site and obtain the two pathways from which the H-cluster can be accessed.

Quantum chemical calculations

Calculations were performed with the model system (see Fig. S9) extracted from the crystal structure of the *Cp* protein (H_{ox} state) and consist of a small diiron subsite $Fe_p^{II}Fe_d^{I}$ linked to the iron-sulfur cubane $[Fe_4S_4]$. Anchoring cysteine residues as well as the proximal cysteine, important

16

in the reaction studied here, were replaced with methenethiols and their carbon atom coordinates were fixed to the crystal positions. In order to compensate a high negative charge of the active site (-3) we included three protonated $CH_3NH_3^+$ molecules at the positions occupied by the lysine residues in the crystal structure. All molecules considered in this study have lowest possible spin state (singlet or doublet) except dioxygen and OOH^+ which have a triplet ground state. Single point energy calculations were performed with B3LYP+D3 functional and the COSMO solvation model to obtain more accurate energy changes and to account for the charge screening by the protein matrix, respectively. For the latter we used a typical dielectric constant of 4, while $\varepsilon = 78$ was used for water. The def2-TZVP basis set was used throughout the study. We note that the selected methodology (moderate amount of the Hartree-Fock exchange in the density functional, large basis set on the sulfur and oxygen atoms as well as a pairwise correction for the dispersion interactions) gives also an accurate description of the isomerisation reactions involving sulfoxygenated species.[57] Further details of the calculations, validation of the density functional against high-level *ab initio* calculations and references relevant to this section can be found in Supplementary section S4. XYZ coordinates of all molecular structures discussed are given in Supplementary section S6.

Authors contributions

References

Refs 51–58 in Supplementary section S7.

[1] Lubitz, W., Ogata, H., Rüdiger, O. & Reijerse, E. Hydrogenases. *Chem. Rev.* **114**, 4081–4148 (2014).

[2] Flanagan, L. A. & Parkin, A. Electrochemical insights into the mechanism of NiFe membrane-bound hydrogenases. *Biochem. Soc. Trans.* **44**, 315–328 (2016).

[3] Fritsch, J. *et al.* The crystal structure of an oxygen-tolerant hydrogenase uncovers a novel iron-sulphur centre. *Nature* **479**, 249–252 (2011).

[4] Volbeda, A. *et al.* Crystal structure of the O_2-tolerant membrane-bound hydrogenase 1 from *Escherichia coli* in complex with its cognate cytochrome *b*. *Structure* **21**, 184-190 (2013).

[5] Hamdan, A. A. *et al.* Relation between anaerobic inactivation and oxygen tolerance in a large series of NiFe hydrogenase mutants. *Proc. Nat. Acad. Sc. USA* **109**, 19916–19921 (2012).

[6] Plumeré, N. *et al.* A redox hydrogel protects hydrogenase from high-potential deactivation and oxygen damage. *Nat. Chem.* **6**, 822–827 (2014).

[7] Fourmond, V. *et al.* Mechanism of Protection of Catalysts Supported in Redox Hydrogel Films. *J. Am. Chem. Soc.* **137**, 5494–5505 (2015).

[8] Fourmond, V. *et al.* The mechanism of inhibition by H_2 of H_2-evolution by hydrogenases. *Chem. Comm.* **49**, 6840–6842 (2013).

[9] Pandey, A. S., Harris, T. V., Giles, L. J., Peters, J.W. & Szilagyi, R. K. Dithiomethylether as a ligand in the hydrogenase H-cluster. *J. Am. Chem. Soc.* **130**, 4533–4540 (2008).

[10] Berggren, G. *et al.* Biomimetic assembly and activation of [FeFe]-hydrogenases. *Nature* **499**, 66–69 (2013).

[11] Silakov, A.; Wenk, B.; Reijerse, E. & Lubitz, W. [14]N HYSCORE investigation of the H-cluster of [FeFe] hydrogenase: evidence for a nitrogen in the dithiol bridge. *Phys. Chem. Chem. Phys.* **11**, 6592–6599 (2009).

[12] Esselborn, J. *et al.* A structural view of synthetic cofactor integration into [FeFe]-hydrogenases. *Chem. Sci.* **7**, 959-968 (2016).

[13] Mulder, D. W. *et al.* Stepwise [FeFe]-hydrogenase H-cluster assembly revealed in the structure of HydA$^{\Delta EFG.}$ *Nature* **465**, 248–251 (2010).

[14] Ghirardi, M. L. Implementation of photobiological H_2 production: the O_2 sensitivity of hydrogenases. *Photosynthesis research* **125**, 383–393 (2015).

[15] Cohen, J., Kim, K., King, P., Seibert, M. & Schulten, K. Finding gas diffusion pathways in proteins: application to O_2 and H_2 transport in CpI [FeFe]-hydrogenase and the role of packing defects. *Structure* **13**, 1321 – 1329 (2015).

[16] Orain, C. *et al.* Electrochemical measurements of the kinetics of inhibition of two FeFe hydrogenases by O_2 demonstrate that the reaction is partly reversible. *J. Am. Chem. Soc.* **137**, 12580–12587 (2015).

[17] Baffert, C. *et al.* Hydrogen-activating enzymes: activity does not correlate with oxygen sensitivity. *Angew. Chem. Int. Edit.* **47**, 2052–2055 (2008).

[18] Stripp, S. T. *et al.* How oxygen attacks [FeFe] hydrogenases from photosynthetic organisms. *Proc. Nat. Acad. Sc. USA* **106**, 17331–17336 (2009).

[19] Stiebritz, M. T. & Reiher, M. Theoretical study of dioxygen induced inhibition of [FeFe]-hydrogenase. *Inorganic chemistry* **48**, 7127–7140 (2009).

[20] Kubas, A., Sancho, D. D., Best, R. B. & Blumberger, J. Aerobic damage of [FeFe] hydrogenases: activation barriers for O_2 chemical attachment. *Angew. Chem. Int. Ed.* **53**, 4081–4084 (2014).

[21] Lambertz, C. *et al.* O_2 reactions at the six-iron active site (H-cluster) in [FeFe]-hydrogenase. *J. Biol. Chem.* **286**, 40614–40623 (2011).

[22] Bruska, M. K., Stiebritz, M. T. & Reiher, M. Regioselectivity of H cluster oxidation. *J. Am. Chem. Soc.* **133**, 20588–20603 (2011).

[23] Finkelmann, A. R., Stiebritz, M. T. & Reiher, M. Activation barriers of oxygen transformation at the active site of [FeFe] hydrogenases. *Inorg. Chem.* **53**, 11890–11902 (2014).

[24] Hong, G. & Pachter, R. Inhibition of biocatalysis in [Fe–Fe] hydrogenase by oxygen: molecular dynamics and density functional theory calculations. *ACS Chem. Biol.* **7**, 1268–1275 (2012).

[25] Swanson, K. D. *et al.* [FeFe]-hydrogenase oxygen inactivation is initiated at the H cluster 2Fe subcluster. *J. Am. Chem. Soc.* **137**, 1809–1816 (2015).

[26] Greco, C. et al. Combining experimental and theoretical methods to learn about the reactivity of gas-processing metalloenzymes. *Energy & Environ. Sci.* **7**, 3543–3573 (2014).

[27] Léger, C.; Dementin, S.; Bertrand, P.; Rousset, M. & Guigliarelli, B. Inhibition and Aerobic Inactivation Kinetics of Desulfovibrio fructosovorans NiFe Hydrogenase Studied by Protein Film Voltammetry. *J. Am. Chem. Soc.* **126**, 12162 – 12172 (2004).

[28] Liebgott, P.-P. *et al.* Relating diffusion along the substrate tunnel and oxygen sensitivity in hydrogenase. *Nat Chem Biol* **6**, 63–70 (2010).

[29] Wang, P.-h. & Blumberger, J. Mechanistic insight into the blocking of CO diffusion in [NiFe]-hydrogenase mutants through multiscale simulation. *Proc. Natl. Acad. Sci. U.S.A.* **109**, 6399–6404 (2012).

[30] Wang, P.-h., Best, R. B. & Blumberger, J. Multiscale simulation reveals multiple pathways for H_2 and O_2 transport in a [NiFe]-hydrogenase. *J. Am. Chem. Soc.* **133**, 3548–3556 (2011).

[31] De Sancho, D., Kubas, A.,Wang, P.-h., Blumberger, J. & Best, R. B. Identification of Mutational Hot Spots for Substrate Diffusion: Application to Myoglobin. *J. Chem. Theory Comput.* **11**, 1919–1927 (2015).

[32] Baffert, C. *et al.* CO disrupts the reduced H-cluster of FeFe hydrogenase. A combined DFT and protein film voltammetry study. *J. Am. Chem. Soc.* **133**, 2096–2099 (2011).

[33] Fourmond, V. *et al.* The oxidative inactivation of FeFe hydrogenase reveals the flexibility of the H-cluster. *Nat. Chem.* **6**, 336–342 (2014).

[34] Cornish, A. J., Gärtner, K., Yang, H., Peters, J. W. & Hegg, E. L. Mechanism of proton transfer in [FeFe]-hydrogenase from *Clostridium pasteurianum*. *J. Biol. Chem.* **286**, 38341–38347 (2011).

[35] Knörzer, P. *et al.* Importance of the protein framework for catalytic activity of [FeFe]-hydrogenases. *J. Biol. Chem.* **287**, 1489–1499 (2012).

[36] Hong, G., Cornish, A. J., Hegg, E. L. & Pachter, R. On understanding proton transfer to the biocatalytic [Fe—Fe] H sub-cluster in [Fe—Fe] H_2ases: QM/MM MD simulations. *Biochim. Biophys. Acta* **1807**, 510–517 (2011).

[37] Long, H., King, P. W. & Chang, C. H. Proton transport in *Clostridium pasteurianum* [FeFe] hydrogenase I: a computational study. *J. Phys. Chem.* B **118**, 890–900 (2014).

[38] Morra, S. *et al.* Site saturation mutagenesis demonstrates a central role for cysteine 298 as proton donor to the catalytic site in CaHydA [FeFe]-hydrogenase. *PloS One* **7**, e48400 (2012).

[39] Morra, S. *et al.* The effect of a C298D mutation in CaHydA [FeFe]-hydrogenase: Insights into the protein-metal cluster interaction by EPR and FTIR spectroscopic investigation. *Biochim. Biophys. Acta* **1857**, 98–106 (2016).

[40] Goldet, G. *et al.* Electrochemical kinetic investigations of the reactions of [FeFe]-hydrogenases with carbon monoxide and oxygen: comparing the importance of gas tunnels and active-site electronic/redox effects. *J. Am. Chem. Soc.* **131**, 14979–14989 (2009).

[41] Dey, S. *et al.* Electrocatalytic O_2 reduction by [Fe-Fe]-hydrogenase active site models. *J. Am. Chem. Soc.* **136**, 8847–8850 (2014).

[42] Wulff, P., Day, C., Sargent, F. &, Armstrong, F. A. How oxygen reacts with oxygen-tolerant respiratory [NiFe]-hydrogenases. *Proc. Nat. Acad. Sc. USA* **111**, 6606–6611 (2014).

[43] Mulder, D.W. *et al.* Investigations on the role of proton-coupled electron transfer in hydrogen activation by [FeFe]-hydrogenase. *J. Am. Chem. Soc.* **136**, 15394–15402 (2014).

[44] Ginovska-Pangovska, B. *et al.* Molecular dynamics study of the proposed proton transport pathways in [FeFe]-hydrogenase. *Biochim. Biophys. Acta* **1837**, 131–138 (2014).

[45] Noth, J. *et al.* Lyophilization protects [FeFe]-hydrogenases against O_2-induced H-cluster degradation. *Scientific reports* **5**, 1-10 (2015).

[46] Fournier, M., Dermoun, Z., Durand, M.-C. & Dolla, A. A new function of the *Desulfovibrio vulgaris Hildenborough* [Fe] hydrogenase in the protection against oxidative stress. *J. Biol. Chem.* **279**, 1787–1793 (2004).

[47] Pandelia, M.-E. E. *et al.* Electronic structure of the unique [4Fe-3S] cluster in O_2-tolerant hydrogenases characterized by ^{57}Fe Mössbauer and EPR spectroscopy. *Proc. Nat. Acad. Sci. USA* **110**, 483–488 (2013).

[48] Stiebritz, M. T. & Reiher, M. Hydrogenases and oxygen. *Chem. Sci.* **3**, 1739–1751 (2012).

[49] Yano, J. *et al.* X-ray damage to the Mn_4Ca complex in single crystals of photosystem II: a case study for metalloprotein crystallography. *Proc. Nat. Acad. Sc. USA* **102**, 12047 – 12052 (2005).

[50] Glasoe, P. K. & Long, F. A. Use of glass electrodes to measure acidities in deuterium oxide. *J. Phys. Chem.* **64**, 188 – 190 (1960).